

Instabilities of longitudinal vortex rolls in katabatic Prandtl slope flows

Cheng-Nian Xiao† and Inanc Senocak

Department of Mechanical Engineering and Materials Science,
University of Pittsburgh, 3700 O'Hara St, Pittsburgh, PA 15261, USA

(Received xx; revised xx; accepted xx)

Stationary counter-rotating longitudinal vortex pairs emerge from one-dimensional Prandtl slope flows under katabatic as well as anabatic conditions due to a linear instability when the imposed surface heat flux magnitude is sufficiently strong relative to the stable ambient stratification. For anabatic flows, these vortices have already been identified to exhibit an unique topology that bears a striking resemblance to speaker-wires since they stay coherent as a single unit without the presence of another vortex pair. Under katabatic conditions and at a constant Prandtl number, we find that the longitudinal vortices emerging at a range of different slope angles possess the similar topology as their anabatic counterparts. We determine the existence of both fundamental and subharmonic secondary instabilities depending on the slope angle for the most likely transverse base flow wavelength. Our results indicate that the most dominant instability shifts from a fundamental to subharmonic mode with increasing slope angle. At shallow slopes, this dynamic contrast with the speaker-wire vortices in anabatic slope flows at the same angle which for which the subharmonic instability is clearly dominant. These modes are responsible for the bending and movement of single or multiple speaker-wire vortices, which may merge or reconnect to lead to dynamically more unstable states, eventually leading to transition towards turbulence. We demonstrate that at sufficiently steep slopes, the dynamics of these vortex pairs are dominated by long-wave reconnections or two-dimensional mergers between adjacent pairs.

1. Introduction

Prandtl's model for katabatic and anabatic slope flows is a popular abstraction used to understand the fundamental characteristics of stably stratified flows in cold weather conditions over non-flat terrains, such as nocturnal winds over hills or katabatic flows over the (Ant-)arctic ice sheets (Prandtl 1942, 1952; Gutman 1983; Zardi & Whiteman 2013). The model can be solved exactly for laminar conditions to obtain buoyancy and velocity solutions that are sinusoidal profiles damped exponentially with increasing height (Shapiro & Fedorovich 2004; Fedorovich & Shapiro 2009). The profiles demonstrate a dominant near-surface along-slope jet which is topped by a weak reverse flow that decays with growing height, as shown in Fig. 1.

In previous investigations, the stability of Prandtl's slope flows and travelling waves along a vertical wall has been studied by Gill & Davey (1969); McBain *et al.* (2007); Maryada *et al.* (2022). We have analyzed the linear stability of katabatic (Xiao & Senocak 2019) and anabatic (Xiao & Senocak 2020) Prandtl slope flows subject to constant surface heat fluxes for inclination angles $2^\circ < \alpha < 70^\circ$ and found the dominating mode to be a stationary longitudinal roll instability at shallow slopes and a traveling wave instability at

† Email address for correspondence: chx33@pitt.edu

slope angles larger than 10° (anabatic) or 70° (katabatic). While the nonlinear travelling wave solutions arising from the corresponding linear mode of the Prandtl slope flows over a vertical wall have been analyzed by McBain *et al.* (2007); Maryada *et al.* (2022), we instead directed our focus to an investigation of the dynamics of longitudinal rolls arising from the primary longitudinal roll instability under anabatic conditions over a shallow slope with $\alpha = 3^\circ$ subject to constant surface heat flux (Xiao & Senocak 2022*b*), which is a novel vortex configuration that has not been studied before. Our prior studies have demonstrated that the vortex instabilities of stably stratified flows are determined by the slope angle α , the transverse vortex spacing b_y , as well as the dimensionless stratification perturbation parameter II_s , which can also be interpreted as the surface heat flux normalized by the background stratification. In this present study, we intend to focus on the dynamics of stationary vortices in katabatic slope flows. In contrast to anabatic slope flows which appear only fleetingly during morning transition before the positive surface heat flux overpowers the surrounding stable stratification, katabatic conditions can be stable and long-lasting as manifested in nocturnal boundary layers or above the (Ant-)arctic ice sheet. Another key difference is the ability of katabatic conditions to support stationary longitudinal vortices emerging from a primary instability at very steep slopes up to 65° (Xiao & Senocak 2019), whereas anabatic conditions do not admit this for slopes larger than 10° (Xiao & Senocak 2020).

Numerous experiments under simpler configurations, i.e. without stratification or surface inclination, have confirmed the emergence and persistence of highly organised two-dimensional (2-D) vortex structures in the course of a developing shear layer downstream of a splitter plate (Winant & Browand 1974; Brown & Roshko 1974). These vortices have been noticed to arise under a multitude of different flow conditions, and appear to be remarkably robust with respect to external disturbances (Wynanski *et al.* 1979). It is evident that any progress in the understanding of turbulent transition will need to accommodate the dynamics and interaction of these large vortex structures. In a seminal work on vortex dynamics, Crow (1970) has studied the linear stability for parallel counter-rotating vortex pairs suspended in quiescent air with neutral stratification and discovered that sinusoidal bending of each individual vortex arises due to a symmetric mode now named after him, which then results to vortex merger and ring formation at precisely those locations where the neighboring vortices approach each other due to bending. This work has been extended by Zheng & Hardin (2017) to include the analysis of anti-symmetric modes in vortex pairs, whereas Crouch (1997) studied the dynamics of two unsteadily tumbling vortex pairs.

For more complicated flow configurations which involve the simultaneous presence of heat transfer, ambient stratification and non-flat surfaces, the scenario outlined above is expected to be insufficient to describe the entire flow physics. However, despite the fact that many real-life phenomena such as geophysical flows contain some or all of these complicating factors, there has been very few attempts to properly comprehend vortex instabilities in these challenging situations.

The role of stratification on Stuart vortices has been studied by Miyazaki & Fukumoto (1992) who showed that elliptic instabilities causing anti-symmetric distortion of vortex cores are suppressed by the presence of stable stratification. However, Le Dizès & Billant (2009) has found that stable stratification can also destabilize a single vertical columnar vortex as a result of resonance with internal gravity waves, which is a so-called radiative instability. Stable stratification can also give rise to a vortex instability in rotating flows called the "zig-zag" instability, first identified and investigated by Billant & Chomaz (2000); Billant (2010). Its formation is due to additional self induction as well as mutual induction between vortices as a result of stratification and rotation that are aligned

with the main vorticity. Its main effect is symmetric bending of individual vortices in co-rotating pairs and anti-symmetric bending in counter-rotating pairs.

Most of the current and ongoing studies on vortex instabilities such as those listed above have implicitly assumed that the main merger dynamics depend on no more than two vortices, which can be either counter-rotating or co-rotating. A notable departure from this tradition is our recent work on the instability of speaker-wire vortices arising in anabatic Prandtl slope flows with surface heating Xiao & Senocak (2022*b*), which required at least two counter-rotating pairs with four vortices to enable vortex mergers or reconnections. This is due to the fact that all fundamental modes are anti-symmetric such that only subharmonic instabilities can move vortices from adjacent pairs closer toward each other. It has been found that the spacing between adjacent vortex pairs is a main factor for determining the strength of the most dominant modes, which is directly correlated to the likelihood of vortex mergers. An intuitive interpretation of the results presented in Xiao & Senocak (2022*b*) is that the further the initial spacing of the base vortices is from that of the most stable configuration, the stronger is the subharmonic instability of the vortex configuration which would cause vortex mergers or the formation of new vortices in order to attain the most optimal vortex spacing. We have also observed in Xiao & Senocak (2022*b*) that *pure* mergers, i.e. the process of fusing two neighboring vortices into a single one without any bending, can be a dominant dynamics due to the fact that the two-dimensional vortex instability is almost as strong as the 3D mode with the maximal possible growth rate.

The present study aims to extend our previous analysis to investigate the dynamics of the longitudinal rolls that emerge as the steady configuration of a linear instability under katabatic conditions at shallow slope angles, i.e. subject to surface cooling. Several distinctions of vortex instabilities under the Prandtl's model sets our work apart from the other aforementioned studies on vortex instabilities such as Crow's instability, elliptic instability, zig-zag instability, and secondary convection rolls. Most significantly, Prandtl's model includes the following key components missing in other configurations: Firstly, a constant ambient stratification that is positioned at an oblique angle to the longitudinal rolls aligned with the main flow direction and secondly, a solid surface wall containing its own boundary layer as part of the Prandtl base flow. Unsurprisingly, the combination of these complicating factors renders a theoretical approach highly difficult and, to the best of our understanding, is not present in the published literature besides our own earlier related work under anabatic conditions. As demonstrated in Xiao & Senocak (2022*b*), the dominant vortex instability in anabatic Prandtl slope flows involves two counter-rotating vortex pairs, also termed *speaker-wire vortices*, thus four individual vortices in total. Following the analysis in Xiao & Senocak (2022*b*), we apply a modal linear bi-global stability analysis to identify different instabilities which can arise from the base flow vortices under katabatic conditions. We will further determine how these instabilities are controlled by external conditions as well as their role in the subsequent transition of slope flows to more unstable configurations.

2. Speaker-wire vortices in katabatic slope flows

2.1. Governing equations and characteristic flow scales

Let us consider the idealised Prandtl slope flow configuration as shown in figure 1a, where α is the slope angle, and gravity \mathbf{g} acts downward in the vertical direction. A constant uniform negative buoyancy flux B_S is imposed at the surface to achieve katabatic

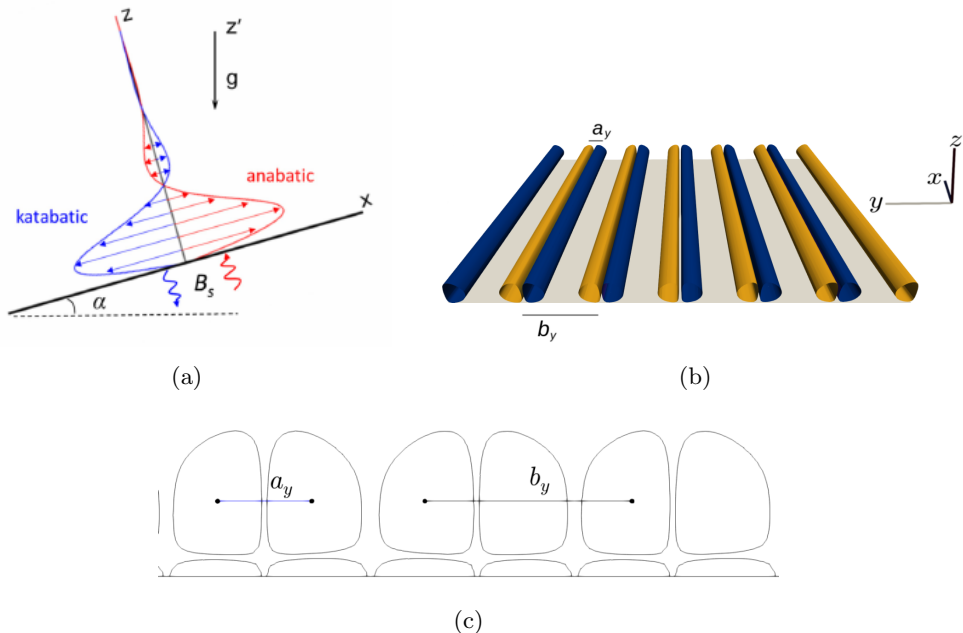


Figure 1: Base flow profiles for slope flows under Prandtl's model: a) Sketch of slope geometry and the rotated coordinate system with 1-D Prandtl slope flow profile; b) Longitudinal vortex pairs (speaker-wire vortices) arising as instability from the 1-D laminar anabatic or katabatic Prandtl slope flow, with definition of coordinate axes, vortex width a_y , and spacing b_y which is equivalent to the transverse wavelength λ_y of the primary longitudinal roll instability; c) cross-slope yz plane with cross-sections of three speaker-wire vortex pairs, indicating of the vortex width a_y and vortex spacing b_y .

conditions. We consider a rotated Cartesian coordinate system whose x axis is aligned with the planar inclined surface. The direction normal to the slope surface is represented by the z axis, whereas the cross-flow transverse direction is aligned with the y coordinate, as shown in Figs. 1a-1b. Let u be the along-slope (longitudinal), v be the cross-slope (transverse), and w be the slope-normal velocity components, such that $\mathbf{u} = u_i = [u, v, w]$ is the velocity vector. The unit gravity vector in the rotated coordinate system is then given by $g_i = (g_1, g_2, g_3) = [\sin \alpha, 0, \cos \alpha]$.

The potential temperature, buoyancy, and the Brunt-Väisälä frequency are denoted by θ, b, N , respectively, where N is related to the ambient potential temperature as $N = \sqrt{\frac{g}{\Theta_r} \frac{\partial \Theta_e}{\partial z'}}$. The buoyancy is defined as a perturbation potential temperature as $b = g(\Theta - \Theta_e)/\Theta_r$, where Θ_r is a reference potential temperature and Θ_e is the environmental (ambient) potential temperature. The kinematic viscosity and thermal diffusivity of the fluid are denoted by ν, β , respectively, and they are assumed to be constant. The transport equations for momentum with a Boussinesq approximation and perturbation buoyancy fields are written as follows:

$$\frac{\partial \mathbf{u}}{\partial t} + \nabla \cdot (\mathbf{u} \otimes \mathbf{u}) = -\frac{1}{\rho} \nabla p + b g \mathbf{n}_\alpha + \nu \Delta \mathbf{u}, \quad (2.1)$$

$$\frac{\partial b}{\partial t} + \nabla \cdot (b \mathbf{u}) = \beta \Delta b - N^2 (\mathbf{n}_\alpha \cdot \mathbf{u}). \quad (2.2)$$

where $\mathbf{n}_\alpha = (\sin \alpha, 0, \cos \alpha)$ is the slope-normal unit vector. The conservation of mass principle is imposed by a divergence-free velocity field

$$\nabla \cdot \mathbf{u} = 0. \quad (2.3)$$

At the surface $z = 0$, a negative buoyancy flux B_s is imposed to generate anabatic flow conditions against a constant stable ambient stratified environment quantified with N^2 .

For the one-dimensional flow problem, Shapiro & Fedorovich (2004) extended the exact solution of Prandtl (1942) to include a constant buoyancy flux at the surface instead of a constant temperature surface condition and introduced the following characteristic flow scales Fedorovich & Shapiro (2009):

$$l_0 = \text{Pr}^{-1/4} \nu^{1/2} N^{-1/2} \sin^{-1/2} \alpha, \quad (2.4)$$

$$u_0 = \text{Pr}^{1/4} \nu^{-1/2} N^{-3/2} B_s \sin^{-1/2} \alpha, \quad (2.5)$$

$$b_0 = \text{Pr}^{3/4} \nu^{-1/2} N^{-1/2} B_s \sin^{-1/2} \alpha, \quad (2.6)$$

where $\text{Pr} = \nu/\beta$ is the Prandtl number. A time scale $t_0 := l_0/|u_0| = \sqrt{\nu\beta} N|B_s|^{-1}$, and a shear scale $S_0 := |u_0|/l_0 = \sqrt{\text{Pr}/\nu} N^{-1}|B_s|$ can also be defined from the above scales. We observe from (2.4)-(2.6) that the length scale characterizing the laminar boundary layer thickness is independent of the surface flux B_s , whereas the magnitude of both the reference velocity and buoyancy scale varies linearly with B_s . Since only the magnitude of the surface buoyancy flux appears in the flow scale definitions, they are the same for both katabatic and anabatic conditions at the same surface buoyancy flux magnitude but with opposite signs. Subsequently, these characteristic scales will be applied to normalize all flow equations and quantities presented herein. Specifically, the dimensionless stratification perturbation number Π_s as introduced in Xiao & Senocak (2019), can be regarded as the imposed surface buoyancy flux B_s normalised by the background stratification scale βN^2 . This unique parameter is determined from the given external flow parameters as follows:

$$\Pi_s \equiv \frac{|B_s|}{\beta N^2}. \quad (2.7)$$

It should be mentioned that the Π_s is not restricted to Prandtl slope flows; it is a necessary additional parameter whenever there exists multiple independent stratification mechanisms. In Xiao & Senocak (2022a), we demonstrated the significance of Π_s as an independent dimensionless parameter in stable open channels flows that are stratified by the simultaneous action of surface cooling as well as a static ambient stratification.

2.2. Steady speaker-wire vortices as longitudinal rolls

The governing flow equations (2.1)-(2.3) can be solved on the 2-D cross-slope yz plane to arrive at the steady longitudinal rolls that arise as a saturated linear instability for slope angles less than 70° when Π_s is sufficiently large Xiao & Senocak (2020). To create the steady vortices that serve as base flows for the secondary stability analysis, the initial flow field is set to be the laminar Prandtl flow profile superposed with a weak sinusoidal disturbance varying along the transverse y direction. For the simulated cross-slope yz plane, the width is chosen to be an integer multiple of the targeted transverse spacing $b_y = \lambda_y$ of the vortex pairs, and the total height of the domain is chosen to be at least $50l_0$. Each length scale l_0 along both the vertical and transverse direction is resolved by at least two mesh points. The evolution of the flow field is simulated until steady state is reached, which happens within a suitable range of Π_s values and results in stationary vortices that are the saturation of the growing linear instability mode. For

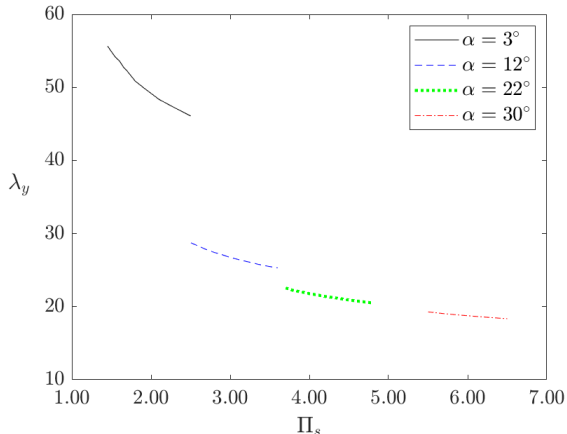


Figure 2: Transverse wavelength of the most dominant linear instabilities for laminar 1-D katabatic Prandtl slope flows at different slope angles α plotted against Π_s .

the spacing of the base vortices, we choose the transverse wavelength λ_y of the most dominant longitudinal roll instability, i.e. the primary mode with the largest growth rate for the one-dimensional Prandtl flow profile. The dependence of λ_y as a function of the stratification parameter Π_s for different slope angles is shown in Fig. 2, which indicates a clear decrease of the transverse wavelength with increasing value of Π_s and slope angle α . Further details about the structure of the vortices that serve as base flow for the secondary stability analysis are provided along with the stability results below.

3. Linear secondary instability analysis of speaker-wire vortices

Let (U, V, W, B) be the 2-D flow profile of the steady longitudinal rolls as computed from Eqn. (2.1)-(2.2), and assuming that modal disturbances to this base flow are of the form

$$\mathbf{q}(x, y, z, t) = \left[\hat{u}(y, z), \hat{v}(y, z), \hat{w}(y, z), \hat{p}(y, z), \hat{b}(y, z) \right] \exp(ik_x x + \omega t),$$

then the equations governing the evolution of the flow disturbances approximated to first order have the following form:

$$ik_x \hat{u} + \frac{\partial \hat{v}}{\partial y} + \frac{\partial \hat{w}}{\partial z} = 0, \quad (3.1)$$

$$\begin{aligned} \omega \hat{u} + iUk_x \hat{u} + \frac{\partial U}{\partial y} \hat{v} + \frac{\partial U}{\partial z} \hat{w} + \frac{\partial \hat{u}}{\partial y} V + \frac{\partial \hat{u}}{\partial z} W \\ = -ik_x \hat{p} - \frac{Pr}{\Pi_s} \sin \alpha \left(-k_x^2 \hat{u} + \frac{\partial^2 \hat{u}}{\partial y^2} + \frac{\partial^2 \hat{u}}{\partial z^2} + \hat{b} \right), \end{aligned} \quad (3.2)$$

$$\begin{aligned} \omega \hat{v} + iUk_x \hat{v} + \frac{\partial V}{\partial y} \hat{v} + \frac{\partial V}{\partial z} \hat{w} + \frac{\partial \hat{v}}{\partial y} V + \frac{\partial \hat{v}}{\partial z} W \\ = -\frac{\hat{p}}{\partial y} - \frac{Pr}{\Pi_s} \sin \alpha \left(-k_x^2 \hat{v} + \frac{\partial^2 \hat{v}}{\partial y^2} + \frac{\partial^2 \hat{v}}{\partial z^2} \right), \end{aligned} \quad (3.3)$$

$$\omega \hat{w} + iUk_x \hat{w} + \frac{\partial W}{\partial y} \hat{v} + \frac{\partial W}{\partial z} \hat{w} + \frac{\partial \hat{w}}{\partial y} V +$$

$$\frac{\partial \hat{w}}{\partial z} W = -\frac{\partial \hat{p}}{\partial z} - \frac{Pr}{\Pi_s} \sin \alpha \left(-k_x^2 \hat{w} + \frac{\partial^2 \hat{w}}{\partial y^2} + \frac{\partial^2 \hat{w}}{\partial z^2} + \hat{b} \cot \alpha \right), \quad (3.4)$$

$$\begin{aligned} \omega \hat{b} + iUk_x \hat{b} + \frac{\partial B}{\partial y} \hat{v} + \frac{\partial B}{\partial z} \hat{w} + \frac{\partial \hat{b}}{\partial y} V + \frac{\partial \hat{b}}{\partial z} W \\ = -\frac{\sin \alpha}{\Pi_s} \left(-k_x^2 \hat{b} + \frac{\partial^2 \hat{b}}{\partial y^2} + \frac{\partial^2 \hat{b}}{\partial z^2} - (\hat{u} + \hat{w} \cot \alpha) \right), \end{aligned} \quad (3.5)$$

where \hat{u} , \hat{v} , \hat{w} , \hat{p} , \hat{b} describe the shape of the flow disturbance along the slope normal and transverse directions, normalised by the flow scales given in (2.4)-(2.6). The normalised base flow field describing the steady vortices is denoted by (U, V, W, B) , and the slope angles studied here are $\alpha = 3^\circ, 12^\circ, 22^\circ, 30^\circ$.

The linearised equations for bi-global stability analysis as shown above can be written as a generalised eigenvalue problem in the following way:

$$A(k_x) \hat{\mathbf{q}}(y, z) = \omega B(k_x) \hat{\mathbf{q}}(y, z), \quad (3.6)$$

The shape of the complex disturbance vector

$$\hat{\mathbf{q}}(y, z) = [\hat{u}(y, z), \hat{v}(y, z), \hat{w}(y, z), \hat{p}(y, z), \hat{b}(y, z)]^T$$

varies in the slope-normal (z) and transverse direction (y), where $(\hat{u}, \hat{v}, \hat{w})$ are the along-slope, cross-slope (transverse) and slope-normal disturbance velocity components. As a bi-global stability analysis, the slope-normal and transverse dimensions are fully resolved and the disturbance variation along the streamwise direction is approximated by only one Fourier mode with wave number k_x . When k_x is zero, then the corresponding mode is 2-D without any streamwise variation, whereas a positive k_x implies a full 3-D disturbance. The appropriate boundary conditions for this problem are no slip for disturbance velocities at $z = 0$ and free-slip at $z \rightarrow \infty$, whereas for the buoyancy disturbance, $\partial \hat{b} / \partial z|_{z=0} = \partial \hat{b} / \partial z|_{z \rightarrow \infty} = 0$ are imposed. The slope-normal derivative of pressure disturbance \hat{p} is also set to zero at both $z = 0$ and $z \rightarrow \infty$. On both transverse boundaries, periodic conditions are imposed for all variables. The generalised eigenvalue problem (3.6) is discretised via spectral elements in the transverse plane, which is available in Nektar++ Cantwell *et al.* (2015). For a base flow containing two full transverse spatial periods, i.e. two speaker-wire vortex pairs, the cross-slope dimension $L_y = 2\lambda_y$ is chosen for the simulation domain; 2 degrees of freedom are used to resolve a unit length scale l_0 in the cross-slope and vertical directions, and the resulting generalised eigenvalue problem are solved with the modified Arnoldi algorithm as implemented in Nektar++. Linear stability of the problem is associated with the real part of the eigenvalues ω , where $\Re\{\omega\} > 0$ represents a positive exponential growth for the corresponding eigenmode, thus an unstable mode. The imaginary part of ω is the temporal oscillation frequency for the corresponding eigenmode, and $\Im\{\omega\} = 0$ represents a stationary mode.

3.1. Instabilities of katabatic speaker-wire vortices at different slope angles

To investigate the secondary linear instability of speaker-wire vortices, eigenvalues with the highest maximal real values for a range of streamwise wave numbers k_x are computed for different stratification perturbation parameters Π_s of the base flow at different slope angles α . The transverse wavelength λ_y of the base flow vortices was chosen to be the most dangerous wavelength at the given Π_s as determined from linear stability analysis of the 1D Prandtl flow profile, which is shown in Fig. 2. Thus in contrast to the study

for vortices under anabatic conditions (Xiao & Senocak 2022b), the focus here is on the effects of the slope angle instead of the vortex spacing. Throughout our analysis, we also assume a constant Prandtl number $Pr = 0.71$ for all the cases.

We observe from Fig. 2 that the slope inclination α exerts a significant effect on the optimal transverse wavelength of the base vortices when all other flow parameters are held constant. Hence, we expect that the secondary instabilities arising from these base flow vortices will also be qualitatively different depending on α . At a given slope angle and Prandtl number, three independent parameters determine the growth rates and oscillation frequencies of the secondary instability, which are the stratification parameter Π_s , the streamwise instability wave number $k_x = 2\pi/\lambda_x$ and the transverse base flow wave number $k_y = 2\pi/\lambda_y$, where $\lambda_y = b_y$ equals the spacing of the base speaker-wire vortex. In the following, we will separately present and discuss the results of the stability analysis for base speaker-wire vortex at four different slope angles α , going from $\alpha = 3^\circ$ to $\alpha = 30^\circ$. The base flow used for modal analysis of each case consists of two speaker-wire vortices arising from the primary linear instability mode, i.e. the transverse domain size is twice the wavelength of the primary vortex instability as described in Xiao & Senocak (2020). This choice of domain size ensures that potential subharmonic eigenmodes with twice the transverse wavelength of the base vortices can be picked up.

3.1.1. Shallow slope: $\alpha = 3^\circ$

At the shallow slope $\alpha = 3^\circ$, it turns out that the transverse spatial period of all the secondary instability modes equals the transverse wavelength λ_y of the base vortices which is also the spacing b_y between the core of adjacent vorte pairs, hence they are all *fundamental* modes. The shape of this mode on the transverse plane is visualized via the contour plot for the streamwise vorticity ω_x as shown in Fig. 3. Thus, this observation is in contrast with the anabatic slope flow at the same angle $\alpha = 3^\circ$ where the most dominant instability is a subharmonic mode Xiao & Senocak (2022b).

Figure 4a shows the growth rates of the most unstable secondary modes as a function of streamwise wavenumbers k_x within the range $[0, 0.15]$ for four different values of stratification parameter $\Pi_s = 1.6, 1.7, 1.8, 1.9$. The growth rate of any mode at any streamwise wavenumber k_x grows with increasing Π_s , which implies a stronger surface cooling for the katabatic slope flow. 2-D modes have zero longitudinal wave number, i.e. $k_x = 0$, and thus only vary on the transverse yz plane but are constant along the streamwise direction.

For the 3-D modes, which have non-zero wave numbers $k_x > 0$, we observe from figure 4a that at large wave numbers $k_x > 0.15$, the growth rates tend to increase with decreasing k_x until reaching a maximal value exceeding the 2-D growth rate ($k_x = 0$) at a optimal wave number $k_x \approx 0.07$, and from that point on they decrease with decreasing wavenumber to reach the 2-D growth rate at $k_x = 0$. In contrast to both the subharmonic and fundamental eigenmodes of speaker-wire vortices under anabatic conditions at the same slope angle of $\alpha = 3^\circ$ (Xiao & Senocak 2022b), the most dominant fundamental modes at katabatic conditions are clearly 3-D since the growth rate of the mode at the optimal non-zero wave number is an order of magnitude larger than that of the zero-wavenumber 2-D mode.

All 3-D fundamental modes with positive longitudinal wavenumbers $k_x > 0$ are oscillatory whose frequency increases monotonically with growing k_x or decreasing wavelength, as shown in figure 4b. The 2-D mode with $k_x = 0$ is stationary, i.e. with zero imaginary part of its eigenvalue. At small streamwise wavenumbers k_x , the oscillation frequencies

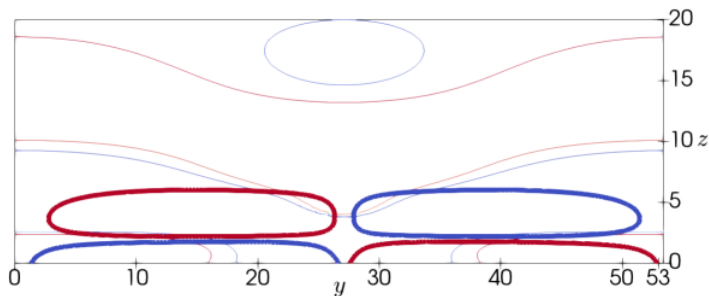


Figure 3: Visualization of streamwise vorticity magnitude for the fundamental mode along with base vortices on cross-slope yz vertical plane in katabatic flow at $\alpha = 3^\circ$ and $\Pi_s = 1.6$ with streamwise wave number $k_x = 0.07$. Thick contour lines represent the base flow, and thin lines are from the instability mode. Contours are drawn at 8% of maximal magnitude in both cases. Only half of the total transverse domain is shown, equalling the transverse wavelength λ_y of the base vortices.

of the 3-D mode decrease to zero with decreasing k_x to converge to the stationary 2-D mode at $k_x = 0$. As figure 4b shows, within the small wave number range, the normalised frequencies of all three cases shown here appear to obey a simple linear dispersion relation given by $\Im(\omega) = \eta \cdot k_x$, where $\eta \approx 0.025$ is empirically determined to fit all three curves. The accuracy of this fit shows that the group speed of the long-wave fundamental vortex instabilities given by $c = \frac{\partial \Im(\omega)}{\partial k_x} = \eta$ is nearly constant and equals $\eta = 0.025$. However, this simple relation no longer holds for modes with wave numbers $k_x > 0.05$ whose oscillation frequencies increase faster than linear with growing wave numbers.

Existence of both 2-D and 3-D fundamental vortex instabilities has also been identified in the study of co-rotating Stuart vortex arrays by Pierrehumbert & Widnall (1982) or as instabilities in a shear layer by Corcos & Sherman (1984), where they are shown to be responsible for the displacement or bending of neighboring vortices. In contrast to the anabatic slope flow at a slope angle of $\alpha = 3^\circ$ (Xiao & Senocak 2022b), there are no subharmonic modes in the katabatic slope flow with angle $\alpha = 3^\circ$. As will be shown later, the fundamental modes for this case as well as at larger slope angles are all anti-symmetric. This suggests that at the initial onset of instabilities, the neighboring vortex tubes will bend and move synchronously in parallel fashion. This is confirmed by direct numerical simulations via solving the full nonlinear governing equations, as shown in the animation available as supplementary movie 1. From the animation, the consistent growth of the anti-symmetric fundamental mode which eventually generates novel structures on top of the original vortices can be seen.

3.1.2. Moderately steep slopes $\alpha = 12^\circ$

At a slope angle of $\alpha = 12^\circ$, both fundamental and subharmonic secondary instabilities are found to emerge. The transverse wavelength of fundamental mode equals the spacing b_y between adjacent base flow speaker-wire vortices, whereas the subharmonic mode have transverse wavelengths twice as large. Hence the additional appearance of the subharmonic mode is a consequence of the increasing slope angle compared to the shallow slope at $\alpha = 3^\circ$.

The shapes of the subharmonic and fundamental modes on the transverse plane are visualized together with the base flow vortices via the contour plot for the streamwise

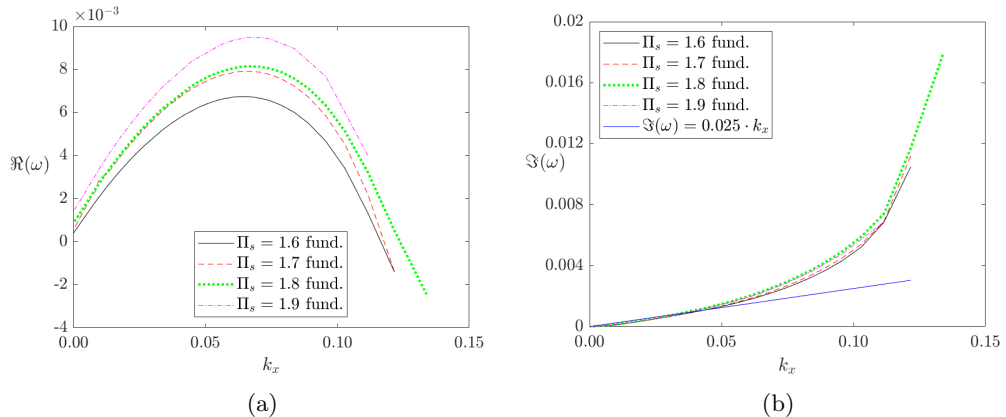


Figure 4: Fundamental modes of katabatic speaker-wire vortices at slope angle $\alpha = 3^\circ$ for different values of Π_s as a function of the longitudinal wave number k_x : Growth rate $\Re(\omega)$ (a) and oscillation frequency $\Im(\omega)$ (b). The linear fit for the dispersion relation between oscillation frequency and streamwise wave number is also shown in (b).

vorticity ω_x as shown in Figs. 5a and 5b. It can be seen that compared to the 3° case as shown in Fig. 3, the base vortices are around half as wide along the transverse direction, but also clearly taller in the vertical. As per definition, the subharmonic modes have a transverse wavelength twice as large as their fundamental counterparts.

Figure 6a presents the growth rates of the most unstable fundamental modes as a function of streamwise wavenumbers k_x within the range $[0, 0.15]$ for four different values of normalized surface heat flux $\Pi_s = 2.6, 2.7, 2.8, 2.9$. The growth rates of the strongest subharmonic modes for streamwise wavenumbers k_x within $[0, 0.03]$ are shown in Fig. 6b. The smaller wavenumber range for the strongest subharmonic modes displayed here implies that their streamwise wavelengths are longer compared to the fundamental modes. For comparison, the growth rate for the strongest subharmonic mode at $\Pi_s = 2.6$ is also displayed together with all the fundamental modes Fig. 6a.

Compared to the shallow slope with $\alpha = 3^\circ$, larger Π_s values are needed to sustain the base vortices that arise as the primary roll instability from the 1D Prandtl slope flow profile (Xiao & Senocak 2019). It is evident from Fig. 6a that a higher value of Π_s , implying a larger normalized surface heat flux magnitude, increases the growth rate of all fundamental modes at any given wave number. However, the same Π_s dependence is not true for the subharmonic modes. As Fig. 6b shows, the growth rate for subharmonic modes attains its maximum at $\Pi_s = 2.7$ and is smaller for larger as well as smaller Π_s values.

From figure 6a, we observe that for modes with sufficiently large wave numbers $k_x > 0.01$, the fundamental mode is stronger than its subharmonic counterpart. The fundamental modes attain the strongest growth at an optimal non-zero wave number k_x between 0.08 and 0.1, and they become monotonically weaker with decreasing wave number below that value. On the other hand, as we observe from figure 6b, the subharmonic modes gain strength with decreasing wave number such that the most dominant mode is purely 2-D at $k_x = 0$. Hence, for very large streamwise wavelengths with $k_x < 0.01$, fundamental modes are weaker than their subharmonic counterparts.

From figure 6c, we observe that all fundamental modes with positive streamwise wavenumbers $k_x > 0$ are oscillatory. For $k_x = 0$, the fundamental modes are all

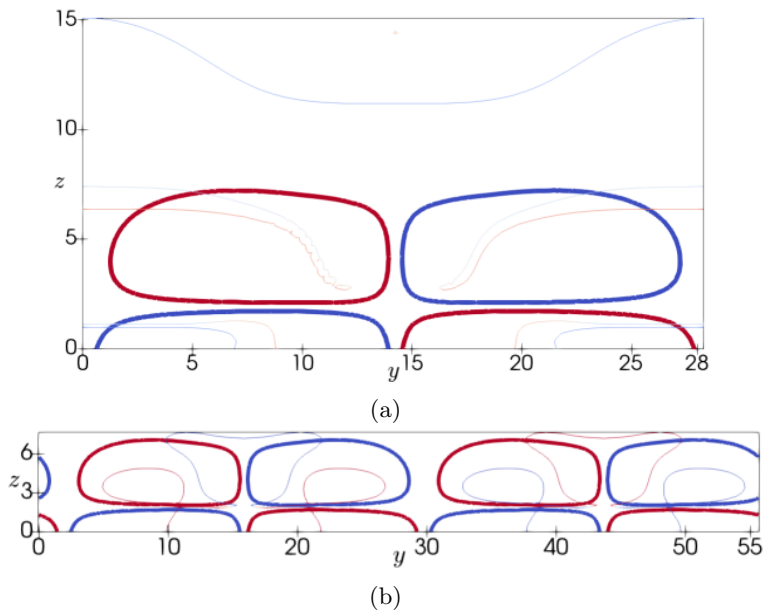


Figure 5: Visualization of streamwise vorticity magnitude for the fundamental mode on cross-slope yz vertical plane in katabatic flow at $\alpha = 12^\circ$ and $\Pi_s = 2.6$: (a) fundamental mode with $k_x = 0.1$; (b) subharmonic mode with $k_x = 0.015$. Thick contour lines represent the base flow, and thin lines are from the instability mode. Contours are drawn at 8% of maximal magnitude in both cases.

stationary, and their frequencies as a function of k_x attains one local maximum in the low-wavenumber range at $k_x \approx 0.004$ and begin to increase with growing wavenumbers for $k_x > 0.012$, as shown in figure 6c. However, at higher wavenumbers beyond $k_x = 0.1$, this trend no longer holds, as the fundamental mode frequencies either stagnate (for $\Pi_s = 2.8, 2.9$) or even slightly decrease (for $\Pi_s = 2.6, 2.7$) with increasing k_x . On the other hand, figure 6d shows that the frequency of subharmonic modes increases monotonically with growing wavenumber. At $k_x = 0$, the 2-D subharmonic mode can be seen to be stationary. As Fig. 6d shows, for wavenumber values less than $k_x = 0.01$, the normalised frequencies for all four Π_s values fit a linear dispersion relation where the group velocity given by $\eta = \frac{\partial \Im(\omega)}{\partial k_x}$ increases with growing Π_s from $\eta = 0.011$ at $\Pi_s = 2.6$ to $\eta = 0.05$ for $\Pi_s = 2.9$. This differs from the behavior of subharmonic modes in anabatic slope flows where the group velocity η remains the same for different Π_s values. Fig. 6d shows that at larger wavenumbers, the linear dispersion relation no longer holds because the oscillation frequencies increase at a faster rate than linear rate with growing wavenumbers for $k_x > 0.01$.

The above-mentioned properties of fundamental and subharmonic modes have significant impact on the dynamics of the base vortices. Since the strongest subharmonic mode is 2-D, we can expect fusion between neighboring vortex pairs instead of wavy reconnections that result in vortex rings like in the Crow instability found in Crow (1970). The fundamental modes which dominate at shorter wavelengths are antisymmetric and will bend each individual vortex parallel to its adjacent neighbors. This co-existence of both dynamics can be seen from animations obtained from direct numerical integration

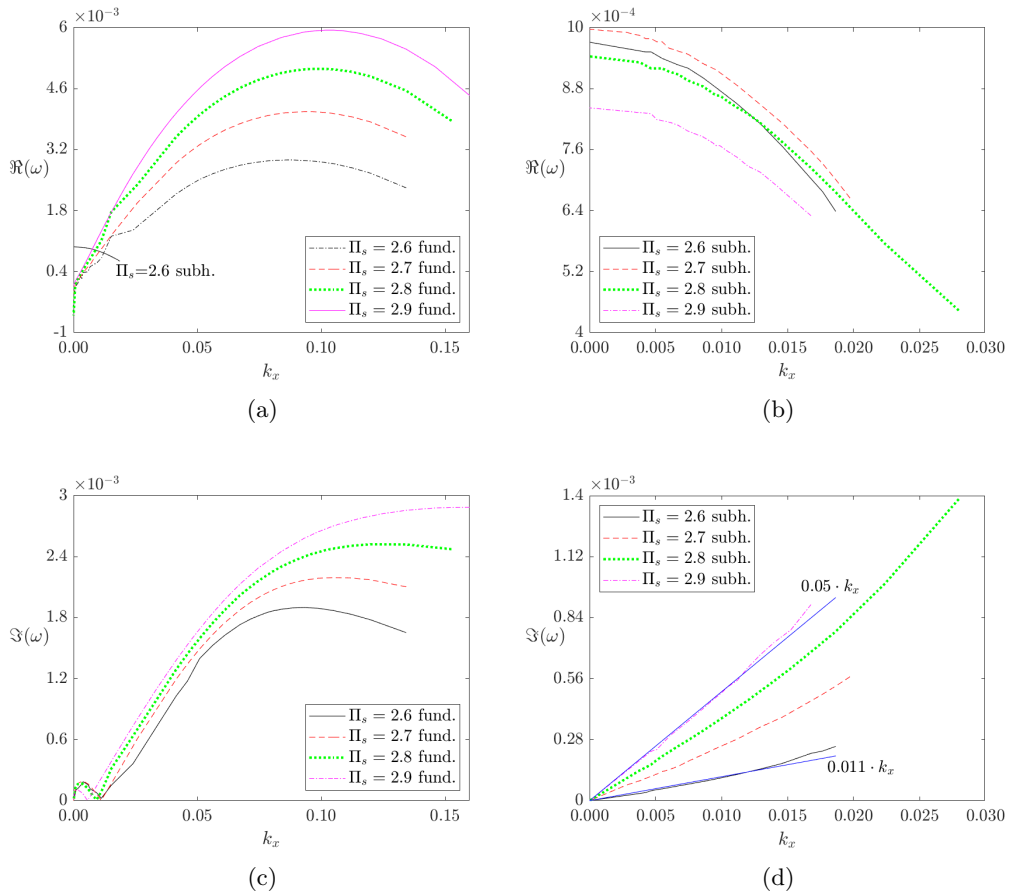


Figure 6: Comparison between fundamental and subharmonic modes of katabatic speaker-wire vortices at slope angle $\alpha = 12^\circ$ for different values of Π_s as a function of the longitudinal wave number k_x : (a)-(b) Growth rates $\Re(\omega)$; (c)-(d) oscillation frequency $\Im(\omega)$. Fundamental modes are shown on the left(a,c), and subharmonic modes are shown on the right(b,d). The linear fit for the relations between oscillation frequency and streamwise wave number of the subharmonic mode is also shown in (d).

of the full nonlinear governing equations as shown in the supplementary movie 2. The animation displays the initial presence of the anti-symmetric fundamental mode which gradually gives way to the subharmonic mode dynamics which moves neighboring vortex pairs closer for mergers.

3.1.3. Steep slopes $\alpha = 22^\circ$

For even steeper slopes with an angle of $\alpha = 22^\circ$, subharmonic and fundamental secondary instabilities again manifest themselves. The typical shapes of these two different kinds of modes on the transverse plane are visualized alongside the base flow vortices via the contour plot for the streamwise vorticity ω_x as shown in Figs. 7a and 7b. Compared to the previous two cases at smaller angles as shown in Fig. 3 and Figs. 5a-5b, the base vortices are narrower along the transverse direction, but also slightly taller in the vertical direction.

The growth rates of the most unstable fundamental modes as a function of streamwise

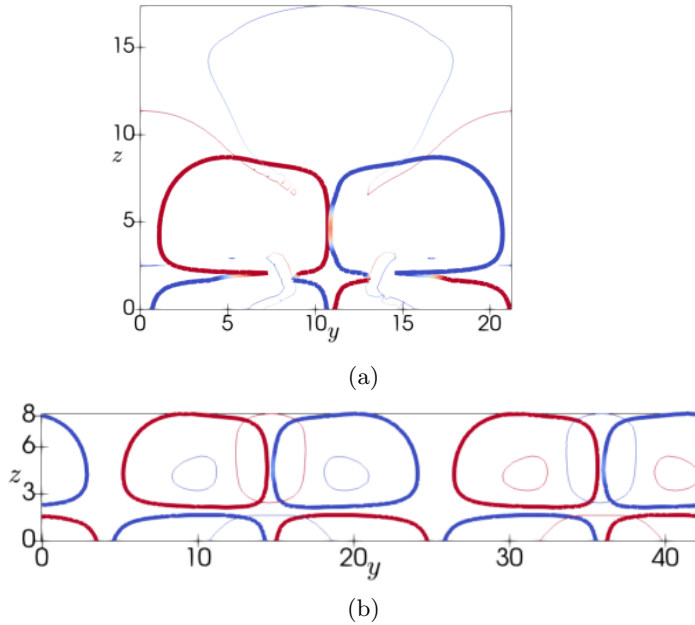


Figure 7: Visualization of streamwise vorticity magnitude for the fundamental mode on cross-slope yz vertical plane in katabatic flow at $\alpha = 22^\circ$ and $\Pi_s = 3.9$: (a) fundamental mode with $k_x = 0.13$; (b) subharmonic mode with $k_x = 0.015$. Subharmonic modes have widths twice as large as fundamental ones. Thick contour lines represent the base flow, and thin lines are from the instability mode. Contours are drawn at 8% of maximal magnitude in both cases.

wavenumbers k_x within the range $[0, 0.2]$ are shown for four different values of normalized surface heat flux $\Pi_s = 3.9, 4.1, 4.3, 4.5$ in figure 8a. Again, a higher Π_s value than at the lower slope angles is needed to trigger and maintain the primary roll instability for the base vortices. The growth rates of the strongest subharmonic modes for streamwise wavenumbers k_x within $[0, 0.04]$ are shown in figure 8b. It can be seen that a higher value of Π_s strengthens all instability modes at any given wave number. By comparing the growth rate plots shown in Figs. 8a and 8b side by side, we observe that the fundamental modes and subharmonic modes are of a similar strength across all wave numbers. The main distinction between the two mode types is the fact that the strongest fundamental mode are 3-D and achieve the highest growth at an optimal non-zero wave number k_x between 0.02 for $\Pi_s = 3.9$ and 0.11 for $\Pi_s = 4.5$, displaying a clear trend of increasing streamwise wavelength with decreasing Π_s value. On the other hand, the subharmonic modes become monotonically stronger with decreasing wave number such that the most dominant mode is purely 2-D at $k_x = 0$, same as in the previously studied slope angles.

All the fundamental modes with non-zero streamwise wavenumbers studied in this case are oscillatory. However, the two-dimensional mode with $k_x = 0$ is stationary. As shown in figure 8c, within the very small wavenumber range $0 < k_x < 0.01$, the frequencies for modes with different Π_s values attain a local maximum at $k_x \approx 0.005$. In the wavenumber range $0.01 < k_x < 0.08$, the fundamental mode frequencies increase with growing wavenumber. However, at higher wavenumbers $k_x > 0.1$, this trend no longer holds, and the frequencies even slightly decrease with increasing k_x . In contrast, figure 8d

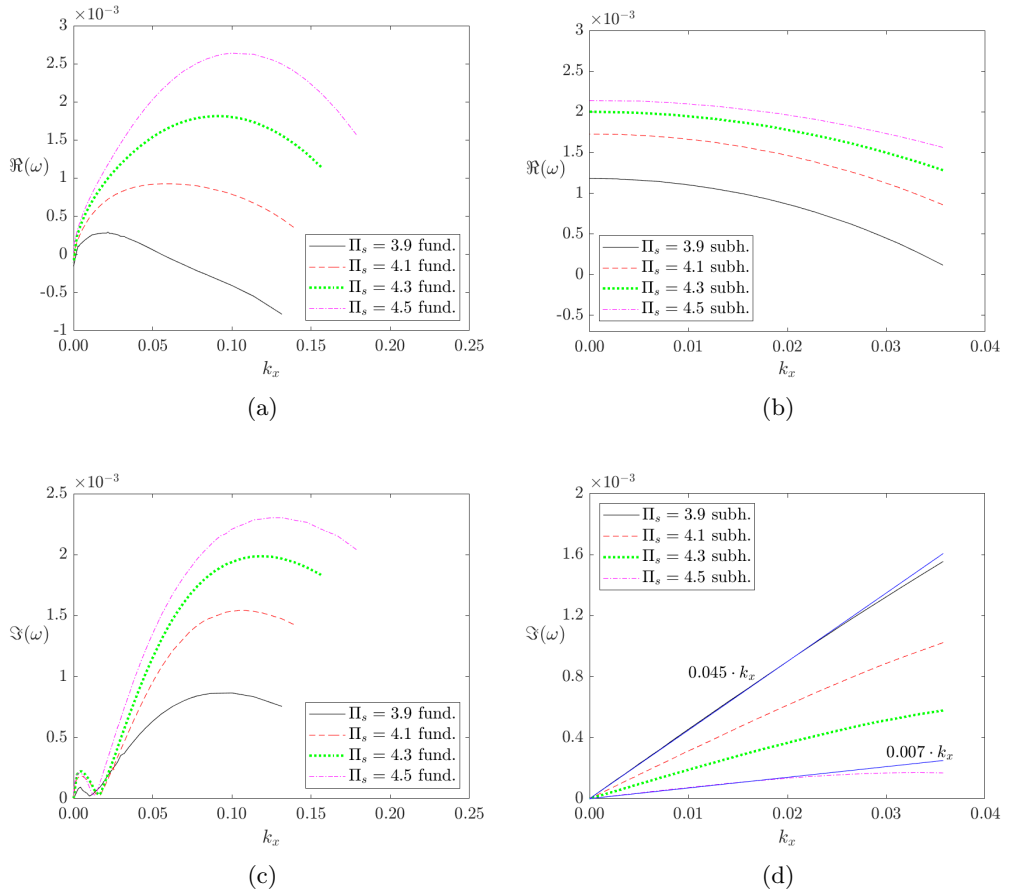


Figure 8: Comparison between fundamental and subharmonic modes of katabatic speaker-wire vortices at slope angle $\alpha = 22^\circ$ for different values of Π_s as a function of the longitudinal wave number k_x : (a)-(b) Growth rates $\Re(\omega)$; (c)-(d) oscillation frequency $\Im(\omega)$. Fundamental modes are shown on the left(a,c), and subharmonic modes are shown on the right(b,d). The linear fit for the dispersion relation of the subharmonic mode is also shown in (d).

indicates that the frequency of subharmonic modes is a monotonically growing function of their wavenumber k_x . All 2-D subharmonic modes ($k_x = 0$) are stationary, and for the low wavenumber range, the frequencies for all four Π_s values can be described via a linear dispersion relation given by $\Im(\omega) = \eta \cdot k_x$. In contrast to the previous case at smaller slope angle, however, the group velocity η decreases with growing Π_s from $\eta = 0.045$ at $\Pi_s = 3.9$ to $\eta = 0.007$ for $\Pi_s = 4.5$. At higher wavenumbers beyond $k_x = 0.03$, the oscillation frequencies of the subharmonic modes start to grow slower than the previous linear rate with increasing wavenumbers.

From these computed properties of fundamental and subharmonic secondary instabilities, we can derive helpful inferences about the dynamics of vortices at the steep slope angle of $\alpha = 22^\circ$. Since the strongest subharmonic mode dominates at lower wave numbers, we can expect long-wave reconnections or pure mergers between neighboring vortex pairs involving four vortices. The fundamental modes which are stronger at shorter wavelengths will bend each individual vortex parallel to its adjacent neighbors. In the full

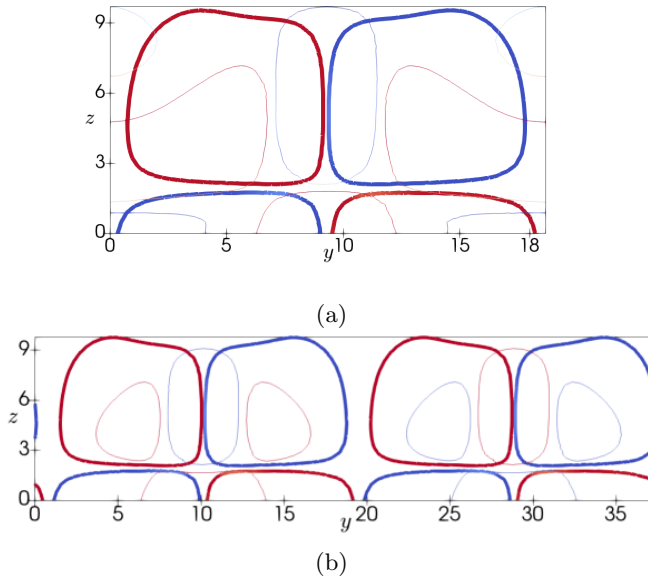


Figure 9: Visualization of streamwise vorticity magnitude for the fundamental mode on cross-slope yz vertical plane in katabatic flow at $\alpha = 30^\circ$ and $II_s = 6.1$: (a) fundamental mode with $k_x = 0.06$; (b) subharmonic mode with $k_x = 0.03$. Thick contour lines represent the base flow, and thin lines are from the instability mode. Contours are drawn at 8% of maximal magnitude in both cases.

nonlinear vortex evolution however, it turns out that the subharmonic modes appear to have a stronger impact on the vortex dynamics than predicted from linear stability analysis, as vortex mergers and reconnections seem to be the dominant feature of such flows with little signature of the wavy bending signature of the fundamental modes. This is very similar to the dynamics at higher slope angles as described below and shown in the animation contained in supplementary movie 3.

3.1.4. Very steep slopes $\alpha = 30^\circ$

The subharmonic and fundamental instabilities of speaker-wire vortices at the steepest slope in this study with $\alpha = 30^\circ$ are visualized together with the base vortices via the contour plot for the streamwise vorticity ω_x on the transverse plane in Figs. 9a and 9b. When compared to the previous cases at smaller angles as shown in Fig. 3, Figs. 5a-5b and Figs. 7a-7b, it can be seen that the base flow vortices continue to shrink along the transverse direction and grow in the vertical with increasing slope angle. As a consequence, the transverse wavelengths of the fundamental and subharmonic modes are also clearly less than that of the modes at lower slope angles.

The growth rates of the most unstable fundamental modes as a function of streamwise wavenumbers k_x within the range $[0, 0.25]$ for four different values of normalized surface heat flux $II_s = 5.5, 5.7, 5.9, 6.1$ are shown in figure 10a. The growth rates of the strongest subharmonic modes for streamwise wavenumbers k_x within $[0, 0.1]$ are shown in figure 10b. Similar like in the previous cases, the strongest subharmonic instabilities have larger streamwise wavelengths than their fundamental counterparts. For sufficiently small

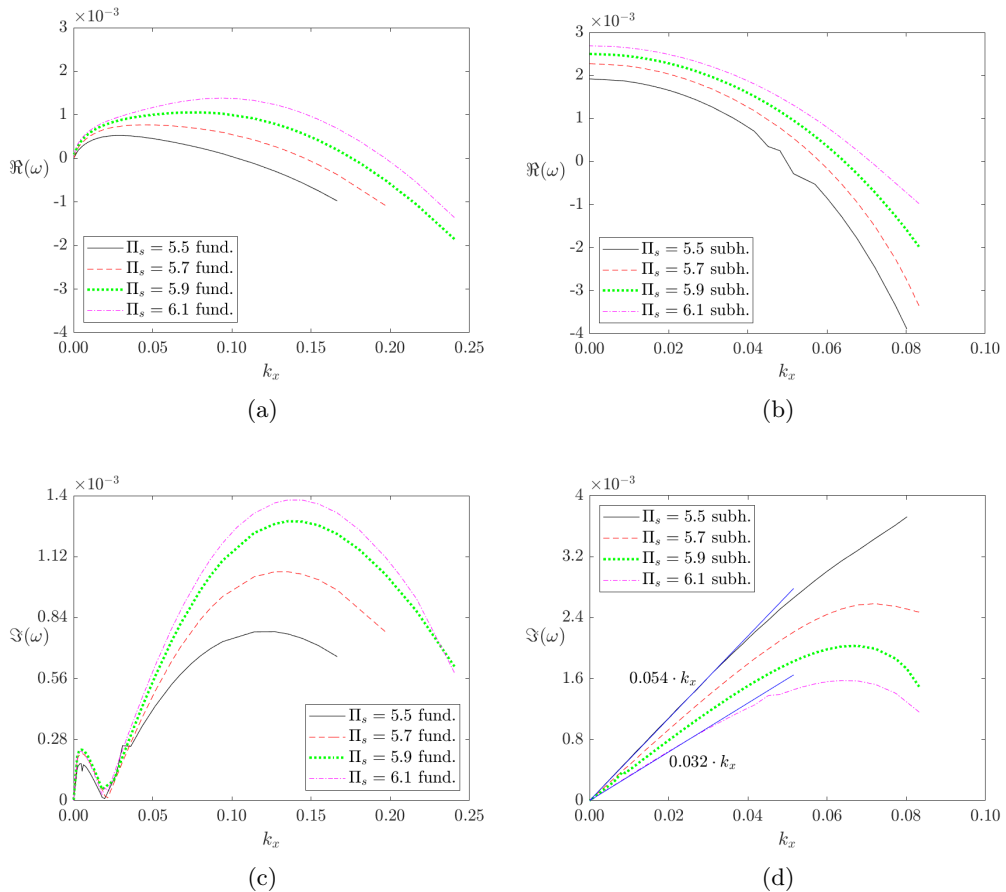


Figure 10: Comparison between fundamental and subharmonic modes of katabatic speaker-wire vortices at slope angle $\alpha = 30^\circ$ for different values of Π_s as a function of the longitudinal wave number k_x : (a)-(b) Growth rates $\Re(\omega)$; (c)-(d) oscillation frequency $\Im(\omega)$. Fundamental modes are shown on the left(a,c), and subharmonic modes are shown on the right(b,d). The linear fit for the dispersion relation of the subharmonic mode is also shown in (d).

wavenumbers, i.e. $0 < k_x < 0.06$, it can be seen that the subharmonic modes are clearly stronger than the fundamental ones, with the distinctively dominating 2-D subharmonic mode at $k_x = 0$. However, since the growth rate of subharmonic modes decays rapidly with growing wavenumber whereas the growth rates of fundamental modes are far less sensitive to wavenumber variation, at sufficiently large wavenumbers $k_x > 0.1$, only the fundamental modes have positive growth rates.

All fundamental modes with non-zero longitudinal wavenumbers $k_x > 0$ are oscillatory; their frequencies are doubly-parabolic functions of k_x with one local maximum in the low-wavenumber range at $k_x \approx 0.01$ and a global maximum at $k_x \approx 0.15$, as shown in figure 10c. On the other hand, figure 10d shows that the frequencies of subharmonic modes have a less complicated relationship to their wavenumbers. All 2-D subharmonic modes ($k_x = 0$) are stationary, and for wavenumber values less than $k_x = 0.04$, the normalised frequencies for all four Π_s values seem to fit a linear dispersion relation given by $\Im(\omega) = \eta \cdot k_x$, where the group velocity is $\eta = 0.054$ for $\Pi_s = 5.5$ and decreases with

growing Π_s to $\eta = 0.032$ at $\Pi_s = 6.1$. However, at larger wavenumbers $k_x > 0.04$, this linear relation no longer holds true. For $\Pi_s = 5.5$, the frequency increases at a smaller rate with growing k_x whereas for the cases with larger Π_s values, the frequency starts to decrease with growing wavenumber when $k_x > 0.06$.

From these properties of fundamental and subharmonic vortex instabilities at the very steep slope, we may infer that 2-D and long-wave subharmonic modes are the dominant driver of vortex dynamics. They would manifest themselves as pure mergers or long-wave reconnections between neighboring vortex pairs. Even though the linear stability results may suggest that the fundamental modes to be visible at shorter wavelengths, in reality, they are overshadowed by the effect of the far stronger long-wave subharmonic modes. This can be seen from animations obtained from direct numerical integration of the full nonlinear governing equations in which the dominating dynamics are vortex mergers and long-wave instabilities, as shown in the animation available as supplementary movie 3.

3.2. Vortex dynamics due to fundamental and subharmonic modes

The role of fundamental instabilities (i.e. modes which have the same transverse spatial period as the base flow) on the dynamics of an array of longitudinal rolls has been extensively documented in previous studies. As an example, they have also been identified as instabilities of Rayleigh-Benard convection rolls which aim at distorting the structure and spacing of the rolls to bring them closer to the optimal wavelength Clever & Busse (1974); Pierrehumbert & Widnall (1982). Other well-known representatives for such modes include the Crow instabilities which are responsible for the bending and reconnection of a vortex pair suspended in quiescent air Crow (1970).

The effect of a fundamental instability on vortices at a slope angle of 12° , which is representative for fundamental modes at other angles as well, is visualised in Fig. 11a. As can be seen, this 3-D fundamental mode causes sinusoidal bending and distortion of each speaker-wire vortex. It is worth noticing that the fundamental modes for speaker-wire vortices are anti-symmetric, i.e. they can only bend both vortices within a pair along the same direction, as shown in Fig. 11a.

Like their fundamental counterparts, 2-D and 3-D subharmonic vortex instabilities which have twice the transverse wavelength as the base flow also play a prominent role in shaping the vortex dynamics, such as in co-rotating Stuart vortex arrays Pierrehumbert & Widnall (1982) or as secondary instabilities in a shear layer by Corcos & Sherman (1984), where they are shown to be responsible for the merging of neighboring vortices. As visualised in Fig. 11b, the 3-D secondary subharmonic modes of the speaker-wire vortices in katabatic slope flows bend adjacent speaker-wire vortices in opposite directions as to facilitate their reconnection in the 3-D case and merger for the 2-D mode. In a recent investigation, the presence of long-wave vortex reconnections associated with the low-frequency content in flow spectra has been observed in the DNS of steep katabatic slope flows with angle $\alpha > 20^\circ$ (Hena-Garcia *et al.* 2023).

We observe from Fig. 11a and 11b that both the fundamental and subharmonic modes are anti-symmetric within a single counter-rotating pair, i.e. they bend the two sister rolls of the same pair along the same direction, thus preventing a vortex reconnection or merger of neighboring vortices within the same pair in contrast to what is observed for a single vortex pair with Crow instability (Crow 1970). This means that a single vortex pair (i.e. a speaker-wire vortex) can remain in its basic pair structure even after the initial onset of instabilities, thus justifying their designation as a coherent vortex structure. Similar vortex structures which remains stable and coherent over long wavelengths have been observed in the *Langmuir vortices* on the surface of seas and

oceans as described in Craik & Leibovich (1976).

As outlined in the previous discussions, the properties of secondary modes for steady speaker-wire vortices are heavily influenced by the size of the slope angle α . This in turn translates into different vortex dynamics at different slope angles. For the four different slope angles $\alpha = 3^\circ, 12^\circ, 22^\circ, 30^\circ$ studied here, our analysis has shown that with increasing values of α , the subharmonic modes become more dominant relative to their fundamental counterparts. At shallow slopes with $\alpha = 3^\circ$, only fundamental modes are supported, whereas at steep slopes with $\alpha > 30^\circ$, the subharmonic modes have the largest growth rates and are clearly stronger than their fundamental counterparts in the low wavenumber range. When α takes on an intermediate value such as between 10° and 20° , both fundamental and subharmonic modes have similar growth rates at stratification parameter II_s not far above the linear stability threshold. To track the further evolution of the vortex dynamics beyond the initial destabilization by the instability modes, we have carried out a series 3-D numerical simulations based on the full nonlinear set of equations (2.1)-(2.3), initializing the flow field with an array of at least 4 base vortex pairs upon which a fundamental or subharmonic mode with 10% of the base flow strength has been added. The simulation domain and boundary conditions for cross-slope yz plane are the same as described in section 2.2, while 32 Fourier modes have been used to resolve the along-slope x direction, which is sufficient for our purpose to study the higher order vortex dynamics before the onset of full turbulence. The animated simulation in supplementary movie 1 shows the initial growth of the fundamental mode in longitudinal rolls at the slope angle $\alpha = 3^\circ$, which later leads to novel structures on top of the original base vortices. Supplementary movie 2 shows the initial vortex dynamics at $\alpha = 12^\circ$ due to the anti-symmetric fundamental mode, which later makes way for a long-wave subharmonic mode that merges two adjacent vortex pairs. The animation shown in supplementary movie 3 illustrates how the subharmonic mode at $\alpha = 30^\circ$ causes vortex reconnections and mergers between rolls from two adjacent pairs, without any apparent signature from a short-wave fundamental mode such as sinusoidal bending of vortices.

3.3. Comparison of secondary vortex modes under katabatic and anabatic conditions

In our earlier work (Xiao & Senocak 2020), we have established that in anabatic slope flows, the stationary roll mode is only the dominant primary instability at slope angle values less than 10 degrees whereas at steeper slopes $\alpha > 10^\circ$, the 2-D travelling wave mode would replace it as the stronger instability. On the other hand, under katabatic slope flow conditions, the stationary longitudinal rolls can emerge naturally as a result of the strongest instability mode over a wide range of slope angles up to 70 degrees. Thus, a comparison between the dynamics of longitudinal rolls under these two conditions is only possible for a narrow range of shallow slopes less than 10° . In this work, the slope angle $\alpha = 3^\circ$ is chosen as the common reference point to contrast anabatic and katabatic slope flows, which is a realistic slope angle that can be observed in actual terrains. For further comparison purposes, we also introduce vortices formed under katabatic conditions at the steep slope angle $\alpha = 30^\circ$.

To illustrate the most significant differences between katabatic and anabatic slope flow conditions, we show the optimal transverse wavelengths of the primary roll instability for the one-dimensional Prandtl flow profile at different slope angles as a function of II_s in Fig. 12a. The aforementioned trend of decreasing vortex spacing with increasing slope angle for katabatic flows is clearly evident, and for both katabatic as well as anabatic conditions, the optimal vortex width decreases with increasing II_s value.

At the shallow slope with angle $\alpha = 3^\circ$ where steady vortices can form under both

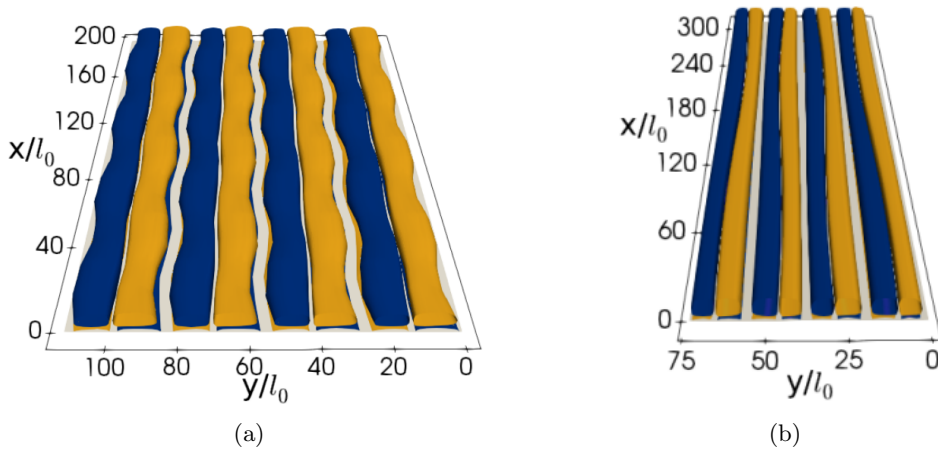


Figure 11: Distortion of longitudinal speaker-wire vortices in katabatic flows due to instabilities: Effect of (a) Fundamental mode at $\alpha = 12^\circ$, $\Pi_s = 2.9$ and (b) subharmonic mode at $\alpha = 30^\circ$, $\Pi_s = 6.1$. Visualization of streamwise vorticity contours at 8% of maximal magnitude for base vortices added with the corresponding instability modes.

katabatic and anabatic conditions, we observe from Fig. 12a that for the same value of $\Pi_s = 1.9$ but with opposite signs of surface heat flux, the transverse wavelength λ_y of the most dominant vortex in the katabatic case is an order of magnitude larger than under anabatic conditions. This observation is visualized in Fig. 12b, which displays the streamwise vorticity contours of both anabatic and katabatic vortices at $\alpha = 3^\circ$, and it is obvious that the vortices formed under katabatic conditions are multiple times wider and taller. Fig. 12b also shows that only at a far steeper slope angle of $\alpha = 30^\circ$ do the katabatic vortices assume a similar size as their anabatic counterparts at $\alpha = 3^\circ$.

The growth rates of secondary vortex instabilities under katabatic and anabatic conditions are displayed in Fig. 13a. For the same slope angle of 3° and stratification parameter $\Pi_s = 1.9$, there are no instability modes for the base vortices at their most preferred width under anabatic conditions, whereas the katabatic configuration is subject to a fundamental secondary instability. Hence, a higher value of $\Pi_s = 2.3$ is chosen for the anabatic slope flow in order to compare its vortex instability against the katabatic conditions at $\Pi_s = 1.9$. As described previously, there exists no subharmonic mode for katabatic vortices at $\alpha = 3^\circ$, whereas the anabatic vortices are susceptible to both fundamental and subharmonic instabilities. Fig. 13a shows that even though the katabatic configuration has a lower Π_s value, its secondary instability exhibits an up to four times larger growth rate than the strongest modes for anabatic vortices. Another key distinction is that the most dominant mode in the katabatic case is clearly 3-D since its highest growth rate at the non-zero optimal streamwise wavenumber is clearly larger than the growth rate of the 2-D mode with zero wavenumber. There is no such behavior in the anabatic case where for both fundamental and subharmonic modes, the largest growth rates are attained at the lowest wavenumbers, and the growth rates remain relatively constant for low wavenumbers. It is interesting to notice that for katabatic vortices at $\alpha = 30^\circ$ which are of a similar size as the anabatic vortices at the shallow $\alpha = 3^\circ$, the growth rates of the fundamental and subharmonic modes at the low wavenumber range are comparable to those under anabatic conditions, which indicates that the size and

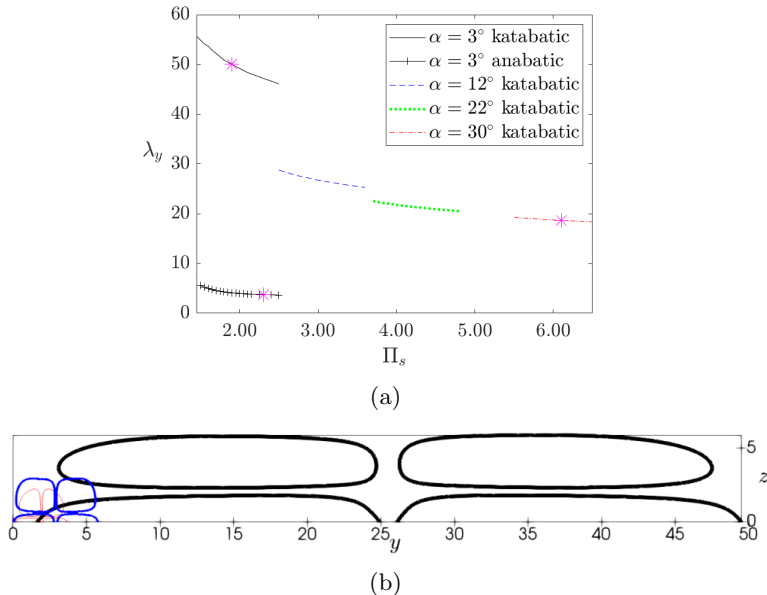


Figure 12: Comparison of the most dominant primary instabilities of Prandtl slope flows under katabatic and anabatic conditions leading to longitudinal rolls, at different slope angles α and as a function of Π_s : (a) transverse wavelength of the most dominant mode, with magenta asterisks indicating cases for which steady vortices have been obtained through numerical simulations; (b) transverse cross-sections of longitudinal speaker-wire vortices arising from 1-D Prandtl flow profile for katabatic and anabatic slope flows at different angles for the three cases marked by asterisks in (a). Reference length scale is chosen to be the value at $\alpha = 3^\circ$ as given in equation (2.4). Streamwise vorticity contour at 12% of respective maximal magnitude is visualized. In (b), thick black lines represent katabatic flow at $\alpha = 3^\circ$, $\Pi_s = 1.9$; medium blue lines represent katabatic flow at $\alpha = 30^\circ$, $\Pi_s = 6.1$, and thin red lines represent anabatic flow with $\alpha = 3^\circ$, $\Pi_s = 1.9$;

shape of the base vortices rather than the slope angle directly exerts a major influence on secondary mode growth for long-wave modes.

The oscillation frequencies of secondary vortex instabilities under katabatic and anabatic conditions are plotted in figure 13b. It is evident that the secondary modes under anabatic conditions have clearly higher frequencies at all wavenumbers than those of modes for katabatic vortices. A major distinction is that while the frequencies of both subharmonic and fundamental modes in the anabatic case fit a linear dispersion relation over the entire range of streamwise wavenumber $0 < k_x < 0.08$, no such simple dependency exists for the frequencies of secondary modes under katabatic conditions which can increase at different rates or even decrease with growing k_x .

4. Conclusions

We carried out a bi-global linear stability analysis to gain insights into the dynamics of longitudinal rolls, a.k.a. speaker-wire vortices, that emerge due to a primary instability from the one-dimensional katabatic slope flows over a range of slope angles. The katabatic conditions are the analogue to the anabatic slope flow conditions, whose effects on vortex dynamics are described in our prior work (Xiao & Senocak 2022b).

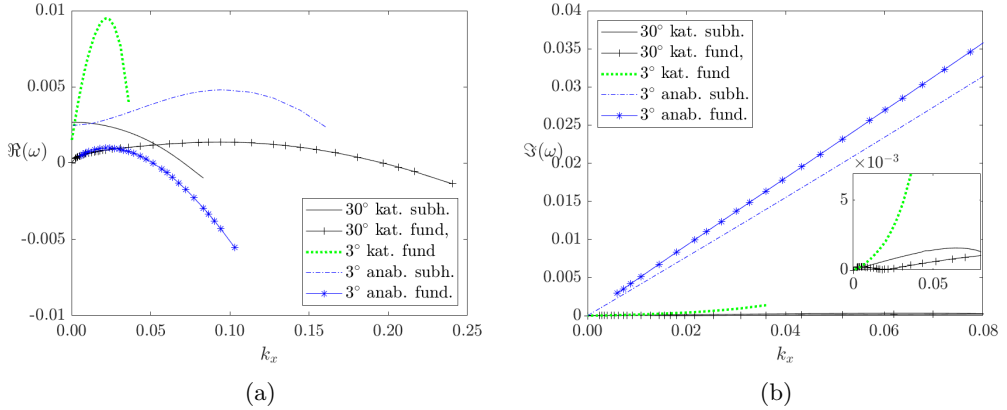


Figure 13: Comparison of instability modes for the longitudinal base vortices under katabatic and anabatic conditions in Prandtl slope flows, at different slope angles α and as a function of streamwise wave number k_x : (a) growth rate; (b) oscillation frequency (inset shows detailed view for katabatic conditions). The values of Π_s are the same for the corresponding vortices as in the previous figure.

Our base flow configuration under katabatic conditions is uniquely different than other well-known counter-rotating vortex pairs (Crow 1970; Billant 2010; Hattori *et al.* 2021; Busse & Clever 1979; Clever & Busse 1974). The katabatic Prandtl slope flow includes an independent background stratification that is at an angle to the cooled solid slope surface. Another unique feature of our configuration is the fact that the stationary longitudinal rolls serving as base flow have three non-zero velocity components even though the flow field is still 2-D, i.e. it only varies along the vertical and transverse dimensions. As a result, it is not too surprising that the instability dynamics of speaker-wire vortices investigated in the current work are distinct from the hitherto known vortex-pair instabilities.

Similar to our earlier investigation of speaker-wire vortices under anabatic conditions, we have established that the counter-rotating vortex pair form a coherent stable unit (i.e. a speaker-wire vortex) that can only lose their individual rolls to mergers or reconnections in the presence of another speaker-wire vortex. Our results for secondary instabilities of speaker-wire vortices have shown that the slope angle α as well as the dimensionless stratification perturbation parameter Π_s , which can be interpreted as a normalized surface heat flux or the strength of the surface thermal forcing relative to the ambient stratification, play a major role in determining which modes are the most significant in destabilizing vortex rolls formed in katabatic slope flows. The major distinction between vortex instabilities in the anabatic and katabatic configurations is the fact that in the latter case, stationary vortices can emerge from the 1D Prandtl base flow profile for all slope angles less than around 70° , whereas this is restricted only to non-steep slopes less than 10° for anabatic slope flows.

For slope angles in the range of $3^\circ - 30^\circ$ at which the 1D katabatic Prandtl slope flow profile is naturally susceptible to the stationary roll mode as primary instability, the most dominant vortex instability shifts from the fundamental mode towards the subharmonic mode with longer streamwise wavelengths with increasing slope steepness. For a shallow slope with $\alpha = 3^\circ$, the only unstable mode is the fundamental instability, no matter how strong the imposed surface heat flux is. This contrasts with vortices in anabatic slope flows at the same angle for which the subharmonic instability is dominant.

For larger slope angles, the subharmonic mode begins to emerge as well. At $\alpha = 12^\circ$, subharmonic mode is still clearly weaker than its fundamental counterpart except at the smallest wave numbers. For even steeper slopes with $\alpha = 22^\circ$, both subharmonic modes and fundamental modes are of comparable strength over a broad range of wave numbers. At the steepest slope angle $\alpha = 30^\circ$ investigated in this work, the subharmonic mode is clearly more dominant than its fundamental counterpart except at the largest wavenumbers. The main difference between the two mode types is that the fundamental instability is a 3-D oscillatory mode whose growth rate at the optimal nonzero streamwise wavenumber is many times larger than the growth rate of the 2-D zero wave number mode. In contrast, the subharmonic mode attains its strongest growth at zero streamwise wavenumber where its oscillation frequency is also zero, hence it is a 2-D stationary mode. This mode exhibits its two-dimensional nature by directly merging two entire rolls from two adjacent but separate speaker-wire vortices without any bending in the streamwise direction.

The 3-D fundamental mode, with a transverse wavelength equivalent to the vortex separation of the base speaker-wire vortices, is anti-symmetric and bends all rolls in all speaker-wire vortices along the same direction, thus the distances between them remain the same as in the original base configuration before the onset of instability. Due to the absence of any symmetric instabilities, the fundamental mode cannot bend the two vortices within a pair towards each other. However, after sufficiently long time, the long-wave or two-dimensional subharmonic instability will eventually manifest itself to move two neighboring speaker-wire vortices from different pairs towards each other, resulting in the merger between two adjacent rolls which are not from the same speaker-wire vortex as in the base configuration as described above.

Our results demonstrate that the only possible vortex merger or reconnection dynamics under Prandtl's katabatic slope flow model is triggered by a long-wave subharmonic mode which requires four vortex rolls in two speaker-wire vortices. In contrast, one single speaker-wire vortex is able to maintain its two-roll structure even after the onset of the fundamental instabilities. The dependence of vortex dynamics on the slope angle is an extension of our earlier study for vortices in anabatic slope flows which focused on the effect of vortex width and separation (Xiao & Senocak 2022*b*). Hence, the vortex dynamics under katabatic conditions investigated in this work are expected to contribute toward a better understanding of turbulent transition in stably stratified boundary layers on non-flat surfaces.

Supplementary movies. 3 Supplementary movies have been attached.

Acknowledgments: This material is based upon work supported by the National Science Foundation under Grant No. (1936445). Research was sponsored in part by the University of Pittsburgh, Center for Research Computing through the computing resources provided.

Declaration of Interests: The authors report no conflict of interest.

REFERENCES

- BILLANT, PAUL 2010 Zigzag instability of vortex pairs in stratified and rotating fluids. part 1. general stability equations. *J. Fluid Mech.* **660**, 354.
- BILLANT, PAUL & CHOMAZ, JEAN-MARC 2000 Experimental evidence for a new instability of a vertical columnar vortex pair in a strongly stratified fluid. *J. Fluid Mech.* **418**, 167–188.
- BROWN, GARRY L & ROSHKO, ANATOL 1974 On density effects and large structure in turbulent mixing layers. *J. Fluid Mech.* **64** (4), 775–816.

- BUSSE, FRIEDRICH H & CLEVER, RICHARD M 1979 Instabilities of convection rolls in a fluid of moderate Prandtl number. *J. Fluid Mech.* **91** (2), 319–335.
- CANTWELL, C.D., MOXEY, D., COMERFORD, A., BOLIS, A., ROCCO, G., MENGALDO, G., GRAZIA, D. DE, YAKOVLEV, S., LOMBARD, J.-E., EKELSCHOT, D., JORDI, B., XU, H., MOHAMIED, Y., ESKILSSON, C., NELSON, B., VOS, P., BIOTTO, C., KIRBY, R.M. & SHERWIN, S.J. 2015 Nektar++: An open-source spectral/hp element framework. *Comput. Phys. Commun.* **192**, 205–219.
- CLEVER, RM & BUSSE, FH 1974 Transition to time-dependent convection. *J. Fluid Mech.* **65** (4), 625–645.
- CORCOS, GM & SHERMAN, FS 1984 The mixing layer: deterministic models of a turbulent flow. part 1. introduction and the two-dimensional flow. *J. Fluid Mech.* **139**, 29–65.
- CRAIK, ALEX DD & LEIBOVICH, SIDNEY 1976 A rational model for Langmuir circulations. *J. Fluid Mech.* **73** (3), 401–426.
- CROUCH, JD 1997 Instability and transient growth for two trailing-vortex pairs. *J. Fluid Mech.* **350**, 311–330.
- CROW, STEVEN C 1970 Stability theory for a pair of trailing vortices. *AIAA J.* **8** (12), 2172–2179.
- FEDOROVICH, E. & SHAPIRO, A. 2009 Structure of numerically simulated katabatic and anabatic flows along steep slopes. *Acta Geophys.* **57** (4), 981–1010.
- GILL, AE & DAVEY, A 1969 Instabilities of a buoyancy-driven system. *J. Fluid Mech.* **35** (4), 775–798.
- GUTMAN, LEV N 1983 On the theory of the katabatic slope wind. *Tellus A* **35** (3), 213–218.
- HATTORI, YUJI, SUZUKI, SHOTA, HIROTA, MAKOTO & KHANDELWAL, MANISH 2021 Modal stability analysis of arrays of stably stratified vortices. *J. Fluid Mech.* **909**.
- HENAO-GARCIA, S., XIAO, C.-N. & SENOCÁK, I. 2023 Investigation of oscillations in katabatic prandtl slope flows. *Q. J. R. Meteorol. Soc.* **149** (750), 247–261.
- LE DIZÈS, STÉPHANE & BILLANT, PAUL 2009 Radiative instability in stratified vortices. *Phys. Fluids* **21** (9), 096602.
- MARYADA, KR, ARMPFIELD, SW, DHOPADE, P & NORRIS, SE 2022 Oblique-mode breakdown of the vertical buoyancy layer. *J. Fluid Mech.* **953**, A34.
- MCBAIN, GD, ARMPFIELD, SW & DESRAYAUD, GILLES 2007 Instability of the buoyancy layer on an evenly heated vertical wall. *J. Fluid Mech.* **587**, 453–469.
- MIYAZAKI, TAKESHI & FUKUMOTO, YASUhide 1992 Three-dimensional instability of strained vortices in a stably stratified fluid. *Physics of Fluids A: Fluid Dynamics* **4** (11), 2515–2522.
- PIERREHUMBERT, RT & WIDNALL, SE 1982 The two- and three-dimensional instabilities of a spatially periodic shear layer. *J. Fluid Mech.* **114**, 59–82.
- PRANDTL, L. 1942 *Führer durch die Strömungslehre*. Vieweg und Sohn.
- PRANDTL, L. 1952 *Essentials of Fluid Dynamics: With Applications to Hydraulics, Aeronautics, Meteorology and other Subjects*. Blackie & Son.
- SHAPIRO, A. & FEDOROVICH, E. 2004 Unsteady convectively driven flow along a vertical plate immersed in a stably stratified fluid. *J. Fluid Mech.* **498**, 333–352.
- WINANT, CLINTON D & BROWAND, FRED K 1974 Vortex pairing: the mechanism of turbulent mixing-layer growth at moderate Reynolds number. *J. Fluid Mech.* **63** (2), 237–255.
- WYGNANSKI, I, OSTER, D, FIEDLER, H & DZIOMBA, B 1979 On the perseverance of a quasi-two-dimensional eddy-structure in a turbulent mixing layer. *J. Fluid Mech.* **93** (2), 325–335.
- XIAO, C.-N. & SENOCÁK, I. 2019 Stability of the Prandtl model for katabatic slope flows. *J. Fluid Mech.* **865**.
- XIAO, C.-N. & SENOCÁK, I. 2020 Stability of the anabatic Prandtl slope flow in a stably stratified medium. *J. Fluid Mech.* **885**.
- XIAO, C.-N. & SENOCÁK, I. 2022a Impact of stratification mechanisms on turbulent characteristics of stable open-channel flows. *J. Atmos. Sci.* **79** (1), 205 – 225.
- XIAO, C.-N. & SENOCÁK, I. 2022b Speaker-wire vortices in stratified anabatic prandtl slope flows and their secondary instabilities. *J. Fluid Mech.* **944**, A27.
- ZARDI, D. & WHITEMAN, C. D. 2013 Diurnal mountain wind systems. In *Mountain Weather Research and Forecasting*, pp. 35–119. Springer.
- ZHENG, Z. C. & HARDIN, J. C. 2017 Importance of antisymmetric modes of the Crow instability. *AIAA J.* **55** (7), 2123–2128.